Theory bridging cell polarities with development of robust complex morphologies

AUTHORS

Silas Boye[1], Steven Rønhild[1], Ala Trusina[1,*], and Kim Sneppen[1,*]

[1] CMOL, Niels Bohr Institute, University of Copenhagen, Blegdamsvej 17, 2100 Copenhagen, Denmark

[*] Correspondence: trusina@nbi.ku.dk and sneppen@nbi.dk

ABSTRACT

Despite continual renewal and damages, a multicellular organism is able to maintain its complex morphology. How is this stability compatible with the complexity and diversity of living forms? Looking for answers at protein level may be limiting as diverging protein sequences can result in similar morphologies. Inspired by the progressive role of apical-basal and planar cell polarity in development, we propose that stability, complexity, and diversity are emergent properties in populations of proliferating polarized cells. We support our hypothesis by a theoretical approach, developed to effectively capture both types of polar cell adhesions. When applied to specific cases of development – gastrulation and the origins of folds and tubes – our theory makes experimentally testable predictions pointing to the strength of polar adhesion, initial and boundary orientation of cell polarities, and the rate of cell proliferation to be major determinants of morphological diversity and stability.

INTRODUCTION

Multicellular organisms are amazing in their ability to maintain complex morphology in face of continuous cell renewal and damages. Adult salamander can regenerate entire limbs (Eguchi et al. 2011), and, during development, some regions can maintain patterning when moved to different parts of an embryo or if the size is varied (Lyons, Kaltenbach, and McClay 2011). Given the vast complexity and diversity of living shapes, how can we reconcile the robustness to perturbations with flexibility to diversify? While undoubtedly the end result is encoded in the DNA and protein networks, looking for an answer at this level is challenging. Examples of phenotypic plasticity (Libby and Rainey 2011), convergent evolution, and contrasting rates of morphological and protein evolution (Cherry et al. 1979) show that morphological similarity may not couple to the protein sequence similarity (Stephen Jay Gould 1970). Inspired by the unfolding of morphological complexity in development, we propose that cellular polarity may be the key for reconciling complexity, robustness, and diversity of organismal morphologies.

During early development the increase in morphological complexity coincides with the progressive polarization of cells – first apical-basal (AB) polarity and then planar cell polarity (PCP) (Müller and Bossinger 2003; Roignot, Peng, and Mostov 2013; Andrew and Ewald 2010; R. Li and Bowerman 2010). This theme is ubiquitous across vertebrates and invertebrates: starting from the single fertilized egg cell, first the morula formed by non-polarized cells turns into the blastula – a hollow sphere of cells with AB polarity. Then, as cells acquire additional PCP, primary head-tail axis forms and elongates during gastrulation and neurulation (Loh, van Amerongen, and Nusse 2016) (Figure 1). Because of the optical

transparency these stages are particularly prominent in sea urchin. At the morula stage, a lumen in the center is formed and is gradually expanding as cells proliferate and rearrange into the hollow sphere. Next, during gastrulation, a group of cells invaginate and rearrange into a tube that narrows and elongates primarily by cell rearrangement and convergent extension movements (Martik and McClay 2017). The tube then merges with the sphere at the side opposite to invagination, and as a result, the sphere transforms into a torus. Emerging data suggest that PCP drives both invagination and tube elongation (Nishimura, Honda, and Takeichi 2012; Croce et al. 2006; Long et al. 2015) – a recurring theme in gastrulation across species.

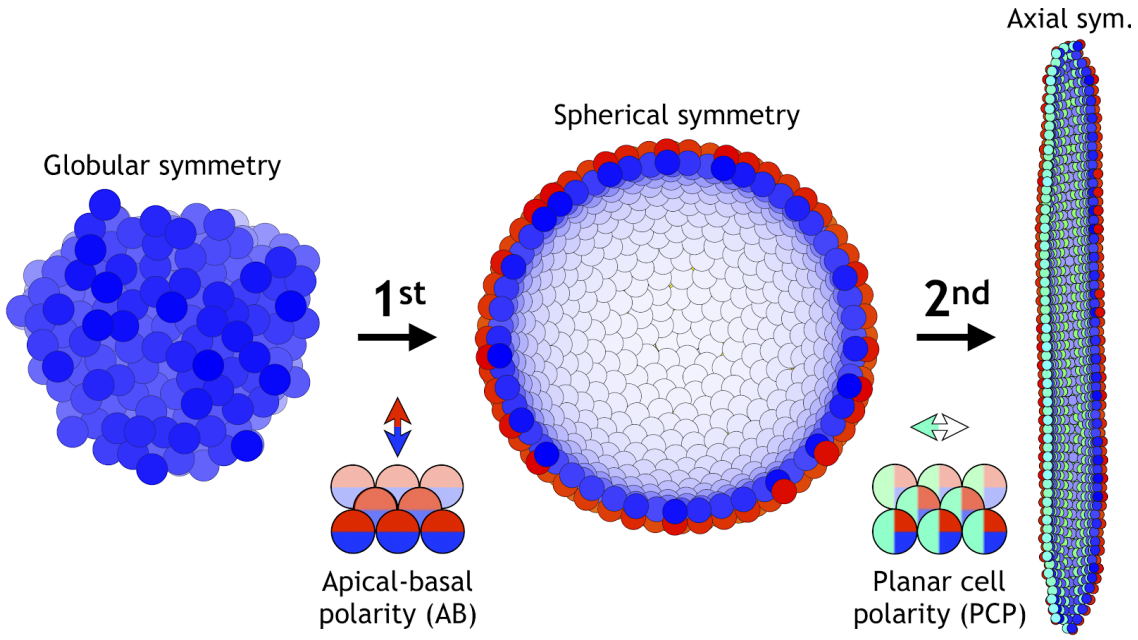

Figure 1. Two symmetry-breaking events, gain of apical-basal polarity and planar cell polarity, on cellular level coincide with the appearance of a rich set of morphologies. Starting from an aggregate of non-polarized cells (globular symmetry), individual cells can gain apical-basal polarity and form one or multiple lumens (spherical symmetry). Additional, gain of planar cell polarity allows for tube formation (axial symmetry). Complex morphologies can be formed by combining cells with none, one, or two polarities.

Mutations in PCP pathways produce shorter and wider tubes (Ochoa-Espinosa, Baer, and Affolter 2012; Saburi et al. 2008; Kunimoto et al. 2017), somites (Song et al. 2010), embryos (Gong, Mo, and Fraser 2004), and also result in neural closure defects (Nishimura, Honda, and Takeichi 2012). Formation and elongation of the tubes can proceed without cell division and cell death by cells rearranging along the tube's axis, termed convergent extension (CE) (Andrew and Ewald 2010; Tanimizu, Miyajima, and Mostov 2009; Martik and McClay 2017). While the importance of PCP in gastrulation and tubulogenesis is well established (Andrew and Ewald 2010; Tanimizu, Miyajima, and Mostov 2009; Martik and McClay 2017; Kunimoto et al. 2017), it is unclear how polarity may control tube stability and dimensions.

The bulk-lumens-folds/tubes transition seen across animal species in early embryogenesis, is also a key feature of the later organ formation. The early stages of organogenesis in liver, kidney, brain, gut, and pancreas are apparently so robust, that they can be recapitulated *in vitro*, allowing for advanced quantification and manipulation (Little 2017). The case of pancreatic organoids is interesting as it illustrates an increase of morphological complexity from spheres to folds. Cells in *in vitro* pancreatic organoids first grow as a bulk and later acquire AB polarity and develop lumens. Depending on the growth conditions organoids develop into a hollow sphere or acquire a complex folded shape (Greggio et al. 2013). It is currently unknown what drives the transition from sphere to folded state; the two main hypothesis are rapid proliferation or physical pressure by growing into a stiff matrigel.

Is the apparent link between cellular polarity and morphological complexity accidental? Or, could it be that morphological transitions, stability, and diversity are emergent features in a population of proliferating polarized cells? If true, can we identify what drives the transition from lumens to folds and tubes? Why are these stable? Can we predict what controls fold depth, and tube length and width? To answer these questions, we lack a unified theory that could bridge polar interactions between single cells to the global features emerging on the scale of thousands of cells in 3D.

Starting with D'Arcy Thompson's seminal contribution (Thompson and Others 1942), quantitative models aided in understanding specific morphogenetic events. Among these are *invagination* (Odell et al. 1981; Rauzi et al. 2015; Polyakov et al. 2014; Hočevar Brezavšček et al. 2012), *primitive streak formation* in gastrulation (Newman 2008), *convergent extension* (Collinet et al. 2015; Belmonte, Swat, and Glazier 2016), *epithelial folding* (Buske et al. 2012; Osterfield et al. 2013; Monier et al. 2015; Murisic et al. 2015), emergence of global PCP alignment from local cell–cell coupling (Amonlirdviman et al. 2005; Le Garrec, Lopez, and Kerszberg 2006; Burak and Shraiman 2009), origins of *tubulogenesis* (Engelberg et al. 2008), and recently statistical properties of branching morphogenesis (Hannezo et al. 2017) (Figure S1). However, they are often on either of the two ends of the spectra: those modeling single cells explicitly, often rely on vertex-based approaches and are limited to dozens of cells (Alt, Ganguly, and Salbreux 2017; Misra et al. 2016; Aigouy et al. 2010; Le Garrec, Lopez, and Kerszberg 2006). To capture the large features spanning thousands of cells, one typically turns to elastic models where AB polarity is implicit and epithelia is presented as a 2D elastic sheet (Hannezo, Prost, and Joanny 2014; Etournay et al. 2015; Hufnagel et al. 2007; Nagai and Honda 2009; Aliee et al. 2012; Nagai and Honda 2001).

We developed a theoretical approach that, with only a few parameters, bridges cellular and organ scales by integrating both types of polarity. A main difference to earlier approaches is that a cell's movement is coupled to how its AB polarity and PCP are oriented relative to each other and relative to neighbor cell polarities. In other words, the adhesion strength between neighbor cells is modulated by the orientation of their polarities. We find that polarity enables complex shapes robust to noise but sensitive to changes in initial and boundary constraints, thus supporting that morphological stability and diversity are emergent properties of polarized cell populations. Lumens, folds, and stable tubes emerge as a result of energy minimization constraints. We make testable predictions on morphological transitions in pancreatic organoids, tubulogenesis, and sea urchin gastrulation. Our approach illustrates the evolutionary flexibility in the regulatory proteins and networks, and suggests that despite differences in proteins between organisms, the same core principles may apply.

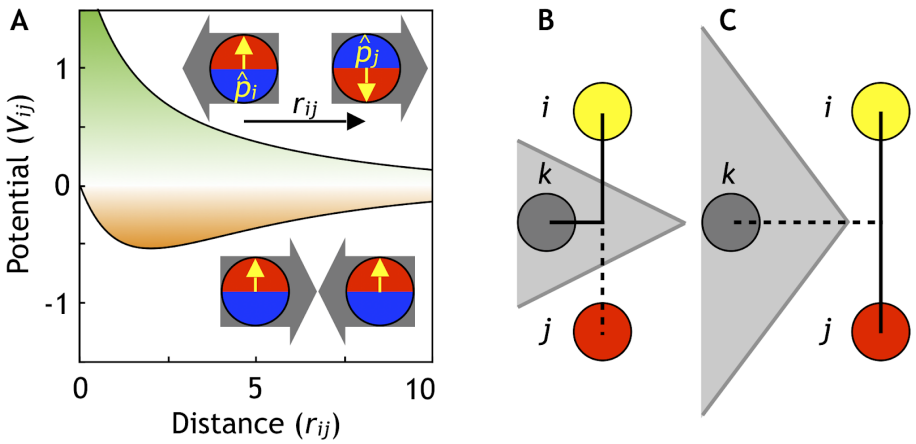

Figure 2. Cells are modeled as interacting particles with a polarity-dependent potential. **(A)** Potential between two interacting cells with apical-basal polarity (see Equation 6). Cells repulse when polarities are antiparallel (top/green part) and attract when they are parallel (orange/bottom part). **(B–C)** Two cells interact only if no other cells block the line-of-sight between them. **(B)** Cell *i* and *j* do not interact if the *ij*'s midpoint is inside of the Voronoi diagram for cell *k* (shaded in grey). **(C)** Cell *i* and *j* interact because cell *k* is further away than the distance *ij*/2 and *ij*'s midpoint therefore lie outside of cell *k*'s Voronoi diagram. See also Figure S2 where we test the sensitivity of our model to the details of the potential and neighborhood assignments.

MODEL

There are three key points that allow us to bridge the scale from cellular level to macroscopic stable morphologies.

(1) Cells are approximated by point particles

Cell–cell adhesion is modeled by repulsive and attractive forces acting between cell centers. This allows a substantially gain in computation time compared to vertex based models where adhesion of cell surface adhesion are explicitly considered (Alt, Ganguly, and Salbreux 2017). The potential for pairwise interaction between two interacting neighbors, *i* and *j*, separated by distance r_{ij} is

$$V_{ij} = e^{-r_{ij}} - S\, e^{-r_{ij}/\beta}, \tag{1}$$

where the the first term corresponds to repulsion and the second term to attraction (see Figure 2A). For a pair of non-polar cells the strength of attraction $S = 1$. $\beta > 1$ is the parameter that sets how much longer the attraction range is compared to repulsion. We set $\beta = 5$ throughout the paper, but our results and conclusions are consistent for smaller β. The main results are also not sensitive to the exact choice of the potential, thus for example the higher power in the exponential,

$$V_{ij} = e^{-(r_{ij})^4} - S\, e^{-(r_{ij}/\beta)^4}, \tag{2}$$

give qualitatively similar results (see Figure S2C). The potential energy of a cell is the sum of pairwise neighbor interactions

$$V_i = \sum_j V_{ij}. \tag{3}$$

(2) Cells interact with (a subset of Voronoi) neighbors

Interacting neighbors of cell *i* are selected from a subset of cells sharing a Voronoi surface. The subset is limited to the nearest neighbors *j* which are closest to the midpoint between *i* and *j* (Figure 2B–C). This constrain effectively corrects for the finite volume associated with point particles and assures that two cells will not interact if the line of sight between their centers is separated by a surface of a third cell. Without this constraint, the macroscopic morphologies collapse. However, our results are robust to replacing the line of sight constraint with full Voronoi and a cut-off distance for attraction force (Figure S2D).

(3) Cells–cell adhesion depends on the orientation of polarity

To capture directional adhesion, we set the strength of attraction, *S*, to be dependent on the relative orientation of the polarities in each of the cells. We assume that AB polarity and PCP are orthogonal, and that the polarities of one cell align with the polarities of it's neighbor cells. Mathematically, we introduce unit vectors, $\hat{p}_i$ and $\hat{p}_j$ representing AB polarity, and $\hat{q}_i$ and $\hat{q}_j$ representing PCP for cell *i* and *j*, respectively. We set

$$S = \lambda_1 S_1 + \lambda_2 S_2 + \lambda_3 S_3, \tag{4}$$

and require that

$$\lambda_1 + \lambda_2 + \lambda_3 = 1, \tag{5}$$

to satisfy the constraint that perfectly aligned cells always have a steady state distance of 2 cell radii (for β = 5). To capture that in an epithelial sheet, AB polarities align parallel to each other and tight adherens junctions form in the plane perpendicular to AB polarity, we introduce the quadruple product

$$S_1 = (\hat{p}_i \times \hat{r}_{ij}) \cdot (\hat{p}_j \times \hat{r}_{ij}). \tag{6}$$

This makes two interacting cells with AB polarity maximally attracted (S_1 = 1) if the two apical sides are next to each other. On the other hand, if apical side of one cell is next to the basal side of another cell, the two cells will be maximally repulsing (S_1 = -1), see Figure 2A. In case of planar polarization, we define

$$S_2 = (\hat{p}_i \times \hat{q}_i) \cdot (\hat{p}_j \times \hat{q}_j), \tag{7}$$

which makes the attraction maximal if the PCP of two cells are parallel to each other and perpendicular to their AB polarities. In addition, we assume that similarly to AB polarity, two cells with PCP are maximally attracted if their PCP are parallel and cells have the same kind of pole (e.g. Vangl-enriched) next to each other,

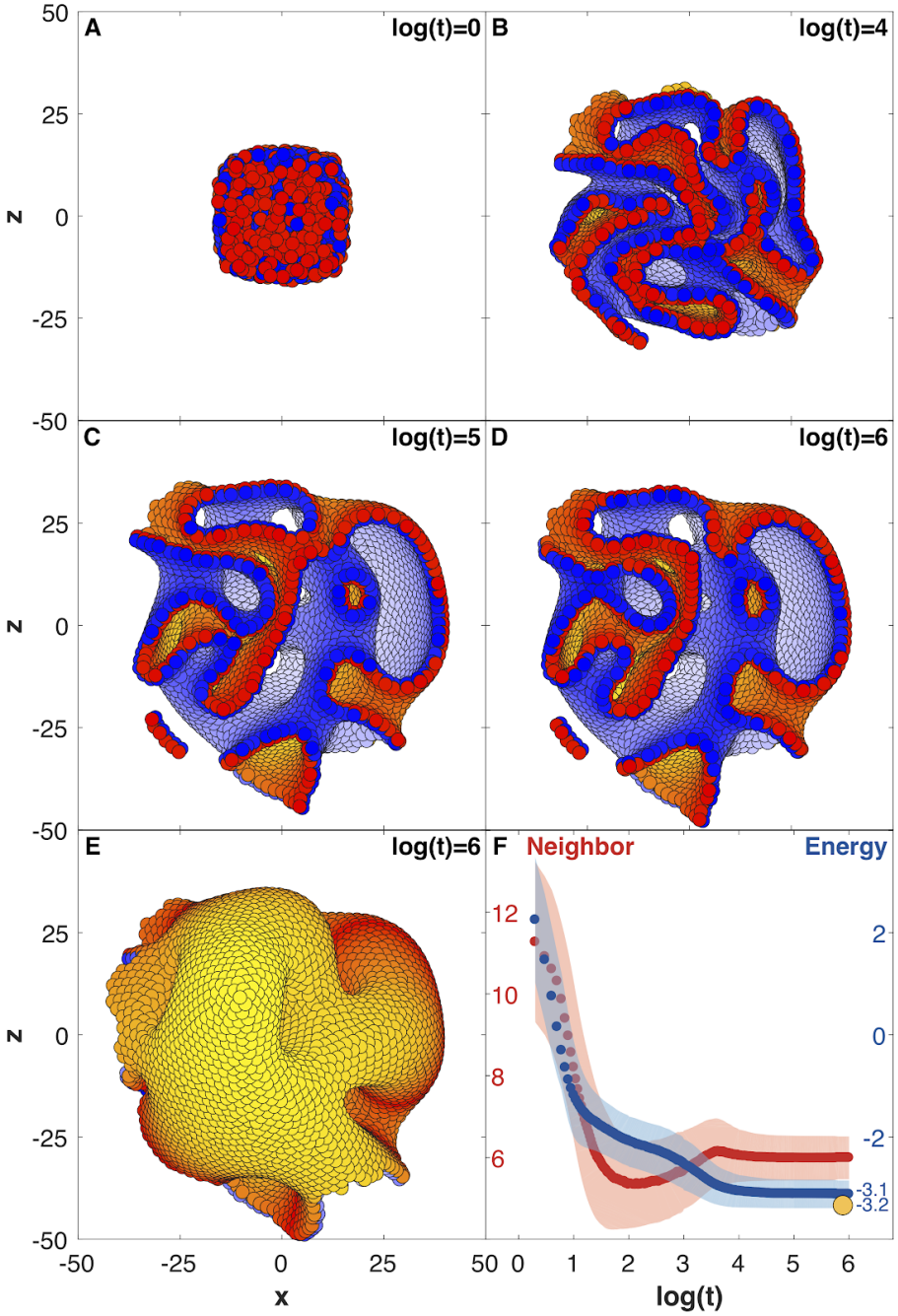

Figure 3. Development of 8000 cells from a compact aggregate starting at time 0. **(A)** Cells are assigned random apical-basal polarity directions and attract each other through polar interactions (see Equation 6). **(A–D)** Cross section of the system at different time points with red and blue marking two opposite sides of the polar cells. Cells closest to the viewer are marked red/blue, whereas cells furthest away are yellow/white. **(E)** Full system at the time point shown in (D). **(F)** Development of the number of neighbors per cell (red) and the energy per cell (blue), as defined by the potential between neighbor cells in Figure 2. Dark colors show the mean over all cells while light-shaded regions show the cell–cell variations. The yellow dot marks the energy for a hollow sphere with the same number of cells. See Movie 1 for full time series.

$$S_3 = (\hat{q}_i \times \hat{r}_{ij}) \cdot (\hat{q}_j \times \hat{r}_{ij}). \quad (8)$$

We later show that this assumption makes neighbor exchange on a sheet possible and results in CE. However, unlike with tight junctions, there is no biological confirmation for preferred directional adhesion with PCP.

The motion of the cells and their polarities are calculated assuming overdamped dynamics $\frac{d\bar{r}_i}{dt} = \frac{dV_i}{d\bar{r}_i} + \eta$, $\frac{d\bar{p}_i}{dt} = \frac{dV_i}{d\bar{p}_i} + \eta$, and $\frac{d\bar{q}_i}{dt} = \frac{dV_i}{d\bar{q}_i} + \eta$ where the $\bar{p}_i$ and $\bar{q}_i$ differentiation takes into account the rotation of polarity vectors, and η is a random uncorrelated Gaussian noise. In practice, we use the Euler method, and perform the differentiation along the polarity by differentiating along all three cartesian coordinates (see Model in the supplementary material). After each time step, we normalize the updated polarity vectors. The above differentiation does not include the change in partners when neighborhood changes. This is treated as a non-equilibrium step where potential energy can increase (Equation 3). Biologically this is similar to cells spending biochemical energy as they rearrange their neighborhood.

The point particle approximation has been utilized earlier for modeling non-polar cell adhesion in early blastocyst (Krupinski, Chickarmane, and Peterson 2011), slug formation in amebae (Dallon and Othmer 2004), and PCP organization in primitive streak formation (Newman 2008). The main novelty of our approach is in the dynamical coupling of cell positions and polarity orientations (Equation 6–8).

RESULTS

We have recently introduced effective representation of AB polarity, and showed that it is sufficient for capturing spherical trophectoderm in the early blastocyst (Nissen et al. 2017). Expanding on that work, we here explore how AB polarity supports diverse yet stable and complex morphologies.

Stable complex shapes emerge from randomly polarized cell aggregates

To test if cellular polarity could enable stable morphologies with lumens and folds as in developing organisms, we first performed a series of tests with AB polarized cells (Figure 3 and Movie 1).

When starting a bulk of cells with AB polarities pointing randomly, an initial rapid expansion (Figure 3A–C) stabilizes into a complex topology of interconnected tunnels (Figure 3C–E). The shape remains unchanged for at least 10 times longer than the initial expansion (Figure 3C–E). The stability of the shape is illustrated by the time evolution of the average energy per cell (Figure 3F) that after an initial fast drop converges to a constant value. As expected, this value is higher than the energy of a hollow sphere (yellow dot in Figure 3F) – a configuration obtained if we start with radially, instead of random, polarized cells and preserve radial polarization at all times. This behaviour is not sensitive to the shape of the potential (Figure S2C) but is sensitive to how the neighborhood is defined (Figure S2D–F). Rerunning the simulation in Figure 3 with different initial conditions results in a different shape (Figures S2A and S3). At the same time the shapes are robust to dynamical noise (Figures S2A–B and S3).

The obtained diversity of metastable topologies suggests a metaphor for evolution of body plans. Diversity and metastability goes hand in hand to create a world of different, yet qualitatively similar shapes. Each could switch into a new distinct geometry by localized changes of a subset of the polarities at the initial state. Thereby, our results support a meta-scale view of evolution where small modifications can lead to large morphological changes, reminiscent of punctuated equilibrium (S. J. Gould and Eldredge 1993).

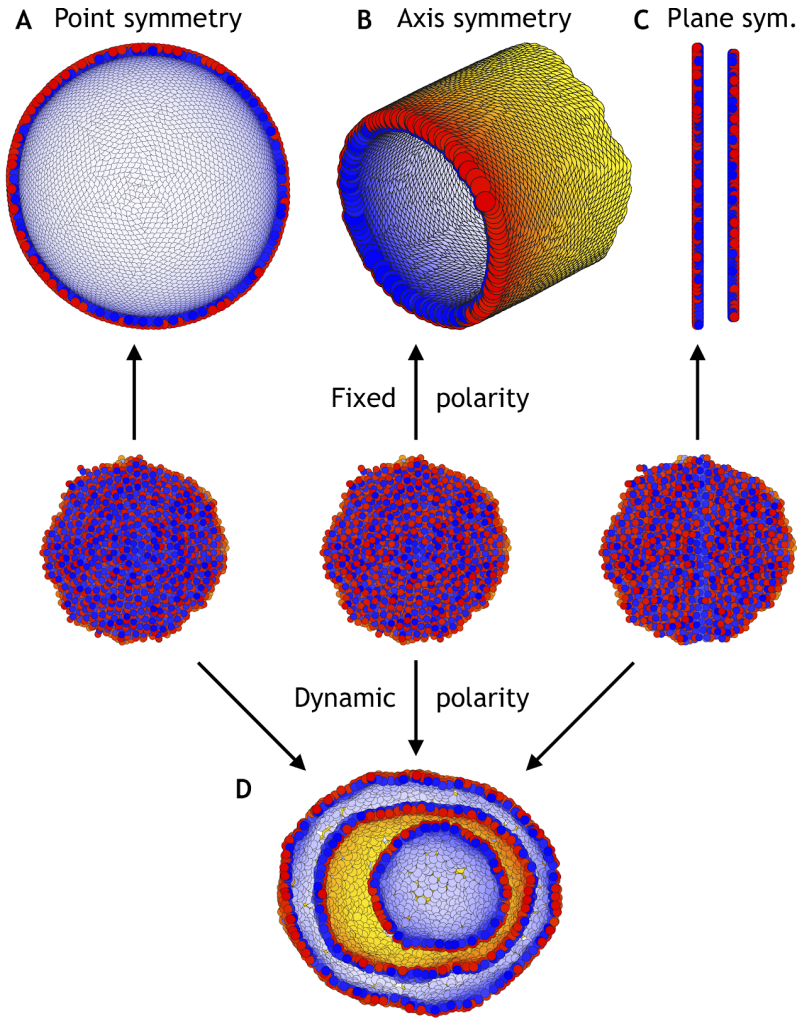

Figure 4. Different topologies can be obtained by varying boundary conditions. **(A)** A hollow sphere emerges if polarities are fixed and initially point radially out from the center of mass. **(B)** A hollow tube is obtained if polarities point radially out from a central axis. **(C)** Two flat planes pointing in opposite directions are obtained if polarities point away from a central plane. **(D)** In all three cases (A–C), if the polarities are allowed to change dynamically and the noise is high, the resulting shape consists of three nested "Russian doll"-like hollow spheres that will never merge due to opposing polarities. See also Figures S2A–B and S3 where we quantitatively study the importance of noise and initial polarities.

The final shapes are robust to noise but sensitive to initial and boundary conditions

To investigate sensitivity to boundary conditions, we consider three cases where polarities are fixed at all times and point either radially out from center of mass (Figure 4A), radially out from a central axis (Figure 4B), or pointing away from a central plane (Figure 4C). As anticipated, the difference in symmetries of boundary conditions result in a sphere, a cylinder, or two parallel planes. At the same time, in these symmetric cases the differences in initial conditions (no boundary conditions) are not sufficient to generate different structures; they all converge to the nested "Russian doll"-like hollow spheres (Figure 4D). In development, this highlights the importance of the neighboring tissues for defining boundary conditions.

Our results thus support the idea that polar adhesion enables stable and robust macroscopic shapes. The closest biological parallels would be the complex luminal morphologies emerging in reaggregation experiments on e.g. *Hydra* (Seybold, Salvenmoser, and Hobmayer 2016) or *in vitro* culture of purjunkie brain cells (Muguruma et al. 2015). Together with our simulations, these experiments highlight how stable and complex topologies can develop in non-proliferating populations from cell rearrangements alone.

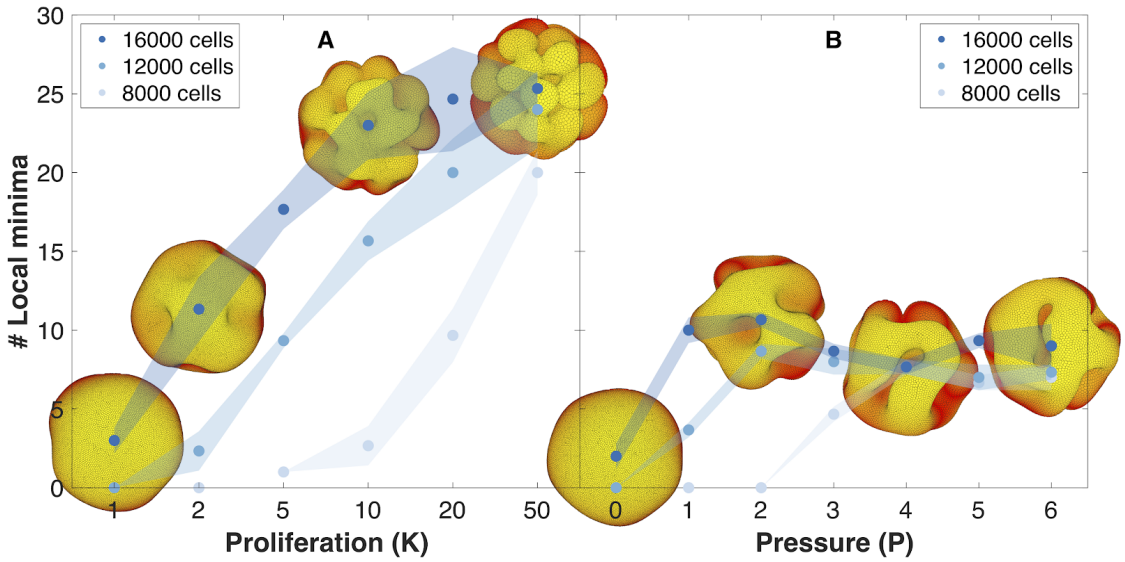

Figure 5. The number of complex folds in a growing organoid depends on the proliferation rate and the pressure from the surrounding medium. **(A)** Number of local minima as a function of proliferation rate, K. *In silico* organoids grow from 200 cells up to 8000, 12000, or 16000 cells with different proliferation rates and no outer pressure. **(B)** Number of local minima as a function of pressure, P. *In silico* organoids grow to the same size with the same proliferation rate $K = 1$ but different outer pressure. The images illustrate the 16.000 cells stage. Blue dots mark the average, while light shaded regions show the SEM based on triplicates. See also Figure S4 for additional measurements on the differences between rapid growth and pressure. In these simulations, two cells do not attract to each other if the angle between their apical-basal polarity is larger than $\pi/2$.

Folding by pressure or rapid proliferation result in different fold-morphologies

Growth is inherent for developing organs (and organisms) and morphological complexity increase with increasing number of cells. *In vitro* pancreatic organoids, started with a few non-polarized cells expand about 50 fold in 7 days. The complexity of the shape correlates with organoid size: small tend to be more spherical but the largest 20 % show folded and branched morphologies reminiscent of pancreas (Greggio et al. 2013).

Transitions from spheres to folded shapes are ubiquitous in 3D organoid systems. Folds are an important part of *in vivo* organ development, and the composition of cell types in the folded organoids is closer to that in real organs (Greggio et al. 2013). To date, it is unclear what drives the transition from spheres to folded lumens. One possibility is that it is driven by the mechanical properties of the matrigel that effectively may place the growing organoid under pressure. Alternatively, data from 3D brain organoids suggests that the rapid cell proliferation leads to the emergence of surface folding (Y. Li et al. 2017).

The simplicity of our tool allows to explore both of these scenarios. To model dividing cells, we pick a random cell from the entire population and introduce a new daughter cell with inherited polarity direction placed in a random location a half cell radius away from the mother cell. This event introduces dynamic perturbation by locally increasing cell density and requires some time to relax back to equilibrium. If proliferation is slow and the time between cell doubling is longer than the relaxation time, the system approaches equilibrium and will expand as a sphere. However, if proliferation is increased, the system will be pushed out of equilibrium and folds will emerge (Figure 5A, Methods).

As cells divide faster, our simulations predict a transition from a smooth spherical shell to an increasingly folded structure with multiple folds and pronounced local maxima, in line with the observation of brain organoids proliferating at different rates (Y. Li et al. 2017). In comparison with the model for cortical convolutions by Tallinen et al. (2016) in which folding is a result of expanding cortical sheet adhered to the non-expanding white matter core, our mechanism does not require a bulk core. Instead folds emerge in a fast expanding sheet when the growth is faster than the global relaxation to dynamical equilibrium.

While we find that the external pressure is not necessary for folding, pressure alone can also drive folding (Figure 5B, Methods). However, this scenario contradicts the observation that pancreatic organoids can grow as spheres or folded morphologies in gels with same stiffness but different media composition (Greggio et al. 2013).

In principle, both scenarios may contribute to folding, but visually the fold morphologies are very distinct. To differentiate between the two, we have quantified the final folded structures in terms of its local minima (Figure 5, Methods). Our simulations predict that in the pressure driven case, the number of local minima does not exceed a upper limit of about 10–12. In the case of out-of-equilibrium proliferation, new folds can continue forming as organoids grow. Increased proliferation causes more and shallower folds. These folds are different than obtained with pressure which causes a shape with fewer but deeper minima. Quantitatively, both the depth and the horizontal extension of the folds are about double as large with pressure than with growth induced folding (Figure S4).

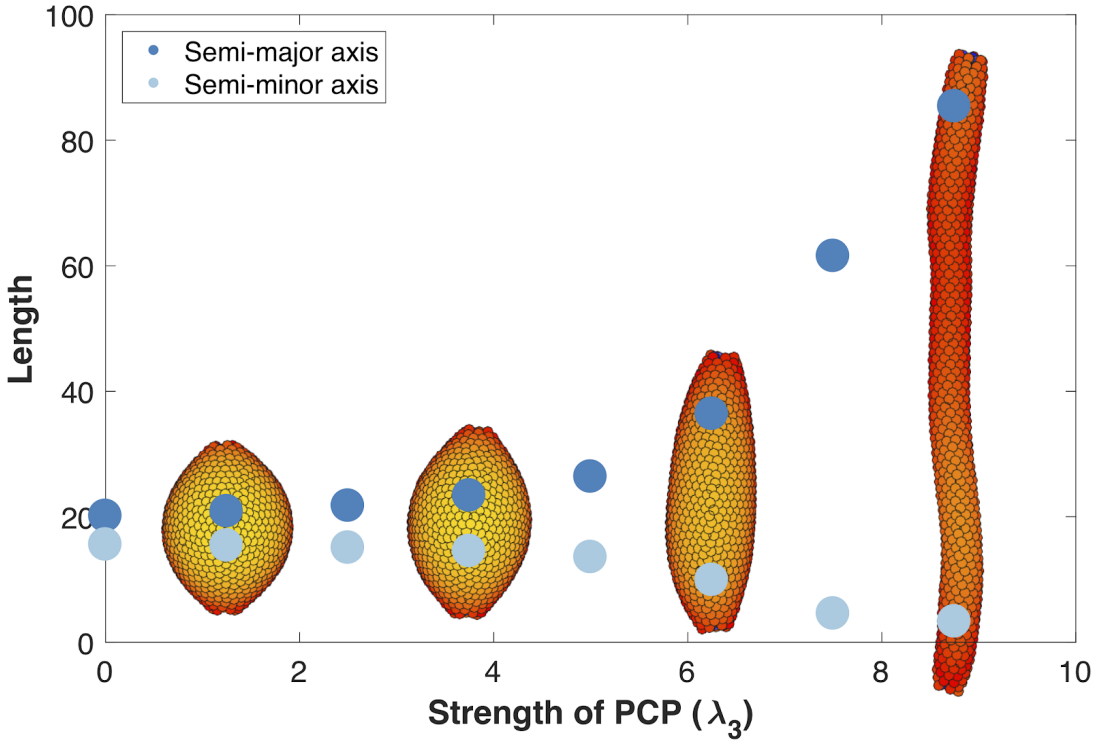

Figure 6. The length and width of tubes are given by the strength of planar cell polarity (PCP, λ_3). For each value of λ_3, we initialize 1000 cells on a hollow sphere with PCP whirling around an internal axis. Semi-major axis (dark blue) and semi-minor axis (light blue) are measured at the final stage (Methods). Images show the final, frozen state. Throughout the figure, $\lambda_2 = 0.5$ and $\lambda_1 = 1 - \lambda_2 - \lambda_3$. The animated evolution from sphere to tube is shown in supplementary Movie 2.

PCP enables convergent extension and robust tubulogenesis

Despite the numerous evidence supporting the role of PCP in tubulogenesis, it remains unresolved whether oriented cell division or the extent of convergent extension controls tube length and width (Karner et al. 2009; Carroll and Yu 2012). It is also debated if it is important for the stability of the tubes, or if it is only important for tube initiation and growth (Kunimoto et al. 2017).

The simplicity of our approach allows us to address these questions by introducing cell–cell interactions through PCP. This term favours front-rear cell alignment in the interaction potential with only two additional parameters: the strength of the orientational constraint of AB polarity and PCP, λ_2, and the strength of PCP, λ_3 (see Equations 4–8). For simplicity, we focus on the stability and tube morphogenesis in systems without cell division.

Inducing PCP in a spherical lumen leads to two significant events. First, independent of initial orientation, after some transient time PCP becomes globally ordered and point around a sphere. This arrangement has the lowest energy state. Second, cells start intercalating along the axis perpendicular to PCP orientation, gradually elongating the lumen (Movie 2). The intercalations along the axis continue until the force balance between AB polarity and PCP is restored at a new equilibrium. Thus, our model predicts that the

strength of PCP (λ_2 together with λ_3) relative to AB polarity (λ_1) determines the width and the length of the tube. Note that this result is very different in nature from the tube presented in Figure 4B as both AB polarity and PCP can now reorient in each cell at any time.

These results support the observations that stable tubes can emerge without cell proliferation. In addition, when first the tube is formed, loss of PCP does not lead to cyst formation as recently shown by Kunimoto et al. (2017). However, localized cysts could result if the lumen is initialized with varying strength of PCP along the axis.

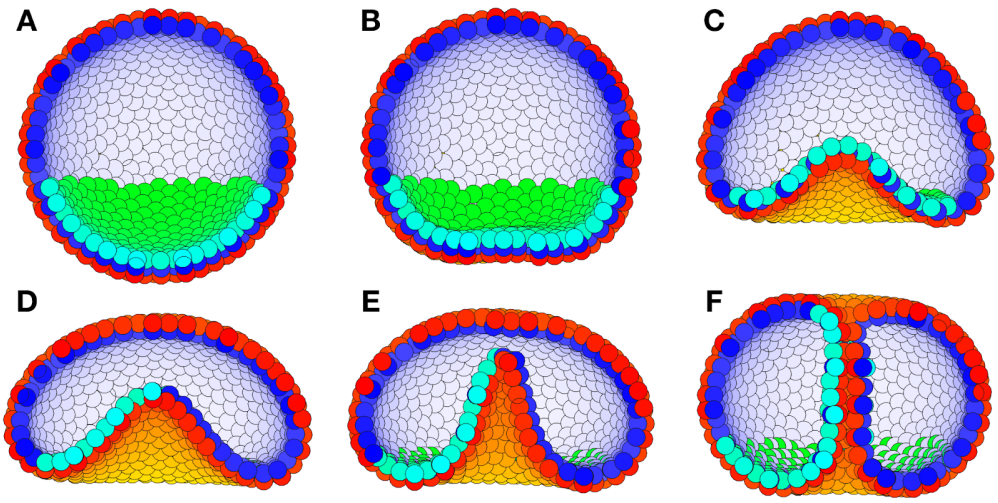

Figure 7. Planar cell polarity (PCP) is sufficient to initiate and drive gastrulation in sea urchin. **(A)** The lower third of the cells in the blastula acquire PCP (green) pointing opposite to the apical-basal (AB) polarity (red–yellow). **(B)** Flattening of the blastula and **(C)** invagination occur if direction of PCP is maintained for some time. During this initial phase $\lambda_2 = 0.1$, and there is no convergent extension ($\lambda_3 = 0$). **(D)** In the final phase, we increase λ_2 to 0.4 and turn on $\lambda_3 = 0.1$. With this, we let PCP relax so it curls around the bottom, and allow it to change dynamically in time. **(E)** As a result, tube narrows and elongates. **(F)** Finally, it connects and merges with the top. The gastrula stabilizes with a tube width that is specified by the strength of λ_3. For full dynamics see Movie 3 in the supplementary material.

Two polarities are sufficient to explain major features of sea urchin gastrulation

Currently invagination in neurulation and gastrulation is understood and quantitatively modeled as a process driven by changes in cell shapes or the mechanical properties of cells with AB polarity (Rauzi et al. 2013; Tamulonis et al. 2011; Misra et al. 2016; Hočevar Brezavšček et al. 2012). This process is often assumed to be driven by apical constriction and decoupled from the eventual tube formation and elongation. However, emerging data suggests that first, apical constriction may not be necessary (Chung, Kim, and Andrew 2017), and second, that PCP drives both invagination and tube elongation (Nishimura, Honda, and Takeichi 2012; Croce et al. 2006; Long et al. 2015).

To probe the limits of our approach, we investigated if AB polarity, PCP, and boundary conditions reminiscent of posterior organizer (Loh, van Amerongen, and Nusse 2016) are sufficient to recapitulate the main stages of sea urchin gastrulation: invagination, tube formation, elongation (by CE), and finally merging of the gastrula tube with the pole opposite to invagination site.

In sea urchin, PCP is likely to be induced in a subpopulation of cells placed as a concentric ring at the site of invagination. PCP is necessary for both invagination and tube extension (Croce et al. 2006). Motivated by this, we assign PCP to all cells in the lower third of the sphere by setting their λ_2 to 0.1 keeping $\lambda_3 = 0$ (Figure 7A, Methods). Further, we assume that PCP initially points toward the center of mass due to signals from the primary mesenchymal cells, a directional constraint that then forces the AB polarity to reorient. As a result of local optimization, cells start rearranging. A subpopulation of cells flatten the bottom (Figure 7B) and bends inward (Figure 7C). At this time point, we allow PCP to relax. When PCP has reached its low energy state (Figure 7D), we increase λ_2 to 0.4, and set $\lambda_3 = 0.1$. The subsequent relaxation to these stronger PCP interactions drives the tube formation (Figure 7E) that elongates and eventually merges with the top of the sphere (Figure 7F and Movie 3). In line with experimental observations, the tube elongates due to cells moving into the tube (Martik and McClay 2017).

The above model leads to a testable prediction: During primary axis formation, local organizing signals (e.g. WNT) (Loh, van Amerongen, and Nusse 2016; J. Wu et al. 2013; Chu and Sokol 2016) orient PCP in cells along the future axis, away from the organizer. As a consequence, we predict that the "wrapping" in neurulation and gastrulation in *Drosophila* (Figure S5) vs. "budding" in sea urchin and organogenesis (Andrew and Ewald 2010; Zegers 2014) are outcomes of different boundary conditions. In both cases, we initiated the process without the use of CE ($\lambda_3 = 0$), but with different initially imposed symmetries. The sea urchin gastrulation was driven by PCP directed toward a point, whereas neurulation (and similarly configured gastrulation in *Drosophila*) was driven by PCP initially directed relative to a line. Thus, we propose that different manifestations of gastrulation reflects different outside constraints on the PCP.

DISCUSSION

Despite the stunning diversity and complexity of morphologies, the same concepts seem to emerge across organismal development. One of them is the link between local, cellular, and global, organs/whole organism, symmetry breaking. We know, from experimental and, to a lesser degree, theoretical work that cellular polarity is essential for forming axis, complex folded sheets, and interconnected tubes (Figure S1). What we do not know is why are these shapes so stable, and where do the differences between species and organs come from. To understand the differences, we typically compare genes or gene regulatory networks, thus limiting ourselves to related processes in a few related species.

Main results

To address the origins of morphological diversity and stability across species and organs, we focused on a phenomenological description of polarized cell–cell interactions. This allowed us to bridge local single cell symmetry breaking events to global changes in morphologies spanning tens of thousands of interacting cells. With this tool at hand, we find that with only a few parameters, we can recapitulate the

two global symmetry breaking events: formation of epithelial sheets and folds by cells with AB polarity, and emergence of global axial symmetry (tubes) among cells with PCP.

Remarkably, our results show that interactions among AB polarized cells lead to metastable topologies, that after initial relaxation remain indefinitely in their final configuration. The topologies are robust to noise, growth, and local damage. These results may explain how organs and embryos preserve their architecture while growing. Polar cell–cell interactions not only provide clue to the morphological stability, but also point to a simple explanation to the origin of the diversity. We find that the exact morphological details are defined by initial conditions, e.g. initial positions and orientation of polarities, and boundary conditions, e.g. fixed polarities for a fraction of the cells in some time. It is thus tempting to speculate that diverse shapes do not require multiple interacting morphogen gradients, but simply can be a result of differences in initial and/or boundary conditions: as for example presence of yolk cells at start and boundary constraints by vitelline membrane (Schierenberg and Junkersdorf 1992; T. Wu et al. 2010).

The diversity of shapes and forms is further enriched by a second symmetry breaking event, PCP, oriented perpendicular to AB axis. Within our phenomenological framework, addition of PCP component is simple, and requires only two additional parameters: one favouring perpendicular orientation of AB polarity and PCP within a cell, and another, favouring parallel PCP alignments between neighbor cells. These constraints are the coarse-grained representation of the well-established experimental and computational results on intracellular symmetry breaking events and global ordering of planar polarities mediated by cell–cell coupling (Le Garrec, Lopez, and Kerszberg 2006; Amonlirdviman et al. 2005; Wang, Badea, and Nathans 2006). The first constraint allowed formation of axial symmetry and in combination with AB polarity, stable tubes. The second constraint resulted in cell rearrangements and intercalations consistent with CE typically associated with PCP. The mechanism of the CE in our model is in line with the results by “filopodia tension model” where elongated structures of many cells emerge from local cell–cell interactions in a direction defined by PCP (Belmonte, Swat, and Glazier 2016).

Combining AB polarization and a local induction of PCP in a subpopulation of cells was sufficient to obtain main stages of sea urchin gastrulation: invagination, tube formation, and elongation through CE as well as merging of the tube with the animal pole at the top of the blastula. By altering the initial and boundary conditions to resemble those of neural plate folding, we, in line with the experimental observations, could obtain transition from an neuroepithelial sheet to a sheet and a tube.

Testable predictions

In addition to our conceptual findings, we arrived to three testable predictions. First, we predict that the two potential mechanisms behind the emergence of folds in pancreatic organoids – matrigel resistance and rapid, out-of-equilibrium, cell proliferation – will result in distinct morphologies. Our results suggest that in case of rapid proliferation, the growing structure will develop many folds close to the surface which later tend to deepen. In contrast, external pressure causes fewer and much deeper folds that form early during growth. Visual inspection of published morphologies seems to support the out-of-equilibrium growth (Greggio et al. 2013; Y. Li et al. 2017). Our model predicts that quantitative measurements of the fold depth and length relative to the size of the growing structure will discriminate between the alternative hypothesis. This can be done in *in vitro* organoids by either phase or confocal fluorescence microscopy

(Greggio et al. 2013; Y. Li et al. 2017). In addition, distributions of cell shapes can be used to asses the out-of-equilibrium growth in 3D organoids (Cerruti et al. 2013).

Our second prediction is that in case of tubes formed by non-proliferating cells, the length and width of the tubes are controlled by the relative strength of AB polarity and PCP. This result calls for quantification of adhesion proteins along the AB and PCP axes. In PCP mutants with shorter and wider tubes one would expect higher fraction of "AB-adhesion" relative to "PCP-adhesion".

Our third testable prediction is on the conditions differentiating between tubes forming perpendicular (e.g. sea urchin gastrulation) or parallel (as in *Drosophila* gastrulation or neurulation) to the plane of epithelium. We predict that the outcome will be defined by the orientation of PCP in the invaginating region and at the boundaries set by e.g. WNT organizing signals. Recent development in imaging localization of PCP complexes in single cells (J. Wu et al. 2013; Chu and Sokol 2016; Minegishi et al. 2017; Habib et al. 2013) allows monitoring localization of PCP complexes, and thus PCP orientation, in individual cells. By placing WNT-soaked (Habib et al. 2013) beads or WNT-secreting cells (Chu and Sokol 2016) one can vary PCP orientation in the cells at the epithelial boundary facing WNT and test for the direction of the tube formation.

Our results open for a series of biological generalizations both in development and diseases. On one hand, we now may be able to explain and unify the apparently very distinct morphological transitions during gastrulation in flies, frogs, fish, mice, and humans by accounting for different initial and boundary conditions. Our model predicts that a moderate change in expression of polarities during some critical evolutionary stages could lead to widely different final morphologies. Thereby, development driven by cell–cell polarity interactions could provide major morphological transitions from local and transient modulations in polarity. This suggests how evolution may bypass larger scale protein evolution to obtain dramatic changes in body plans.

On the other hand, it becomes possible to think of gastrulation, neurulation, tubulogenesis, and organogenesis as the same class of phenomena, where the orientation of the tube is guided by local organizers, and lengths/widths of the tubes are determined by the relative strength of AB polarity and PCP. At the same time, there is an emerging view that wound healing and cancer are local perturbations – e.g. local loss of cells, dysregulation of cell polarities (Martin-Belmonte and Perez-Moreno 2011), proliferation, or autonomously induced organizing signals – of otherwise conceptually the same developmental processes (Humphries and Mlodzik 2017). The power of our here presented tool is that it allows to quantitatively address these hypothesis through predictive models for the dynamics of many cells that interact through combinations of AB polarity and PCP.

METHODS

Throughout the paper, we use the Euler method to integrate the ordinary differential equations stated in the Model section with dt set to 0.1 or 0.2. Lower dt values will give qualitatively similar results but with increased simulation time. Higher dt values, will result in a collapse of the presented morphologies.

The noise parameter $\eta = 10^{-4}$ where nothing else is stated. Lower noise values will give more smooth simulations, while η on the order of 10^{-1} will result in collapsing shapes (see also Figure S2A–B).

Proliferation rate in growing organoids

In Figure 5, the number of cells, N, at a given time, t, is given by $N = 200 \exp(Kt)$ where K is the growth rate. For reference, the timescale in Figure 5 is a factor thousand slower than the timescale in Figure 3.

Modeling resistance from matrigel

In Figure 5, we model resistance from the matrigel by imposing a surface force pointing towards the center of mass. The potential of the pressure in the growth medium is given by $V_M = -Pr^2/r_{\max}$ where P is the stiffness of the medium, r is distance from the center of mass, and $r_{\max}$ is the distance to the cell that is the furthest away from the center of mass. The resulting force will be constant in time at the periphery. Thus, all cells on a growing sphere will be exposed to a force of equal size. However, cells that end up deep inside a folded morphology will experience weaker resistance.

Quantification of the local minima

In Figure 5, the number of local minima is defined as the number of cells that do not have any neighbor cells that are closer to the center of mass than themself, and at the same time have an average angle between their AB polarity and their neighbor cells displacement vector that is less than $\pi/2$.

Measuring the tube length and width

In Figure 6, the semi-minor and semi-major axes correspond to the half-width and half-length of the tubes, respectively. As cells on opposite sides of a tube have AB polarity pointing in opposite directions, we approximate the semi-major and semi-minor axes, by finding the half of the maximum and minimum distance between two cells with AB polarity pointing in opposite directions.

Modeling cells with different polarities

In Figure 7, each cell is assigned a specific value of polarity strengths ($\lambda_{1,i}$, $\lambda_{2,i}$, and $\lambda_{3,i}$). We define the mutual interaction strength between a pair, i and j, of cells in Equation 4 with different polarity strengths by setting $\lambda_1 = \max(\lambda_{1,i}, \lambda_{1,j})$, and $\lambda_2 = \min(\lambda_{2,i}, \lambda_{2,j})$ as well as $\lambda_3 = \min(\lambda_{3,i}, \lambda_{3,j})$. This choice makes sure that two neighbor cells interact with a force with equal magnitude but opposite sign. The maximum for λ_1 is chosen to keep a steady-state distance of 2 cell radii between perfectly aligned cells. The pairwise average between polarity strengths will give qualitatively similar results.

ACKNOWLEDGEMENT

We would like to thank Anne Grapin-Botton for insightful discussions on organoids. This research has received funding from the Danish National Research Foundation (grant number: DNRF116) and the European Research Council under the European Union's Seventh Framework Programme (FP/2007 2013)/ERC Grant Agreement n. 740704.

DECLARATION OF INTERESTS

The authors declare no competing interests.

REFERENCES

Aigouy, Benoît, Reza Farhadifar, Douglas B. Staple, Andreas Sagner, Jens-Christian Röper, Frank Jülicher, and Suzanne Eaton. 2010. "Cell Flow Reorients the Axis of Planar Polarity in the Wing Epithelium of Drosophila." *Cell* 142 (5): 773–86. https://doi.org/10.1016/j.cell.2010.07.042.

Aliee, Maryam, Jens-Christian Röper, Katharina P. Landsberg, Constanze Pentzold, Thomas J. Widmann, Frank Jülicher, and Christian Dahmann. 2012. "Physical Mechanisms Shaping the Drosophila Dorsoventral Compartment Boundary." *Current Biology: CB* 22 (11): 967–76. https://doi.org/10.1016/j.cub.2012.03.070.

Alt, Silvanus, Poulami Ganguly, and Guillaume Salbreux. 2017. "Vertex Models: From Cell Mechanics to Tissue Morphogenesis." *Philosophical Transactions of the Royal Society of London. Series B, Biological Sciences* 372 (1720). https://doi.org/10.1098/rstb.2015.0520.

Amonlirdviman, Keith, Narmada A. Khare, David R. P. Tree, Wei-Shen Chen, Jeffrey D. Axelrod, and Claire J. Tomlin. 2005. "Mathematical Modeling of Planar Cell Polarity to Understand Domineering Nonautonomy." *Science* 307 (5708): 423–26. https://doi.org/10.1126/science.1105471.

Andrew, Deborah J., and Andrew J. Ewald. 2010. "Morphogenesis of Epithelial Tubes: Insights into Tube Formation, Elongation, and Elaboration." *Developmental Biology* 341 (1): 34–55. https://doi.org/10.1016/j.ydbio.2009.09.024.

Belmonte, Julio M., Maciej H. Swat, and James A. Glazier. 2016. "Filopodial-Tension Model of Convergent-Extension of Tissues." *PLoS Computational Biology* 12 (6): e1004952. https://doi.org/10.1371/journal.pcbi.1004952.

Burak, Yoram, and Boris I. Shraiman. 2009. "Order and Stochastic Dynamics in Drosophila Planar Cell Polarity." *PLoS Computational Biology* 5 (12): e1000628. https://doi.org/10.1371/journal.pcbi.1000628.

Buske, Peter, Jens Przybilla, Markus Loeffler, Norman Sachs, Toshiro Sato, Hans Clevers, and Joerg Galle. 2012. "On the Biomechanics of Stem Cell Niche Formation in the Gut--Modelling Growing Organoids." *The FEBS Journal* 279 (18): 3475–87. https://doi.org/10.1111/j.1742-4658.2012.08646.x.

Carroll, Thomas J., and Jing Yu. 2012. "Chapter Eight - The Kidney and Planar Cell Polarity." In *Current Topics in Developmental Biology*, edited by Yingzi Yang, 101:185–212. Academic Press. https://doi.org/10.1016/B978-0-12-394592-1.00011-9.

Cerruti, Benedetta, Alberto Puliafito, Annette M. Shewan, Wei Yu, Alexander N. Combes, Melissa H. Little, Federica Chianale, et al. 2013. "Polarity, Cell Division, and out-of-Equilibrium Dynamics Control the Growth of Epithelial Structures." *The Journal of Cell Biology* 203 (2): 359–72.

https://doi.org/10.1083/jcb.201305044.

Cherry, L. M., S. M. Case, J. G. Kunkel, and A. C. Wilson. 1979. "Comparisons of Frogs, Humans, and Chimpanzees." *Science* 204 (4391): 435. https://doi.org/10.1126/science.204.4391.435.

Chu, Chih-Wen, and Sergei Y. Sokol. 2016. "Wnt Proteins Can Direct Planar Cell Polarity in Vertebrate Ectoderm." *eLife* 5 (September). https://doi.org/10.7554/eLife.16463.

Chung, Seyeon, Sangjoon Kim, and Deborah J. Andrew. 2017. "Uncoupling Apical Constriction from Tissue Invagination." *eLife* 6 (March). https://doi.org/10.7554/eLife.22235.

Collinet, Claudio, Matteo Rauzi, Pierre-François Lenne, and Thomas Lecuit. 2015. "Local and Tissue-Scale Forces Drive Oriented Junction Growth during Tissue Extension." *Nature Cell Biology* 17 (10): 1247–58. https://doi.org/10.1038/ncb3226.

Croce, Jenifer, Louise Duloquin, Guy Lhomond, David R. McClay, and Christian Gache. 2006. "Frizzled5/8 Is Required in Secondary Mesenchyme Cells to Initiate Archenteron Invagination during Sea Urchin Development." *Development* 133 (3): 547–57. https://doi.org/10.1242/dev.02218.

Dallon, John C., and Hans G. Othmer. 2004. "How Cellular Movement Determines the Collective Force Generated by the Dictyostelium Discoideum Slug." *Journal of Theoretical Biology* 231 (2): 203–22. https://doi.org/10.1016/j.jtbi.2004.06.015.

Eguchi, Goro, Yukiko Eguchi, Kenta Nakamura, Manisha C. Yadav, José Luis Millán, and Panagiotis A. Tsonis. 2011. "Regenerative Capacity in Newts Is Not Altered by Repeated Regeneration and Ageing." *Nature Communications* 2 (July): 384. https://doi.org/10.1038/ncomms1389.

Engelberg, Jesse A., Minji Kim, Keith E. Mostov, and C. Anthony Hunt. 2008. "In Silico Simulation of Epithelial Cell Tubulogenesis." In *2008 30th Annual International Conference of the IEEE Engineering in Medicine and Biology Society*, 1036–39. IEEE. https://doi.org/10.1109/IEMBS.2008.4649336.

Etournay, Raphaël, Marko Popović, Matthias Merkel, Amitabha Nandi, Corinna Blasse, Benoît Aigouy, Holger Brandl, et al. 2015. "Interplay of Cell Dynamics and Epithelial Tension during Morphogenesis of the Drosophila Pupal Wing." *eLife* 4 (June): e07090. https://doi.org/10.7554/eLife.07090.

Gong, Ying, Chunhui Mo, and Scott E. Fraser. 2004. "Planar Cell Polarity Signalling Controls Cell Division Orientation during Zebrafish Gastrulation." *Nature* 430 (7000): 689–93. https://doi.org/10.1038/nature02796.

Gould, S. J., and N. Eldredge. 1993. "Punctuated Equilibrium Comes of Age." *Nature* 366 (6452): 223–27. https://doi.org/10.1038/366223a0.

Gould, Stephen Jay. 1970. "Evolutionary Paleontology and the Science of Form." *Earth-Science Reviews* 6 (2): 77–119. https://doi.org/10.1016/0012-8252(70)90027-9.

Greggio, Chiara, Filippo De Franceschi, Manuel Figueiredo-Larsen, Samy Gobaa, Adrian Ranga, Henrik Semb, Matthias Lutolf, and Anne Grapin-Botton. 2013. "Artificial Three-Dimensional Niches Deconstruct Pancreas Development in Vitro." *Development* 140 (21): 4452–62. https://doi.org/10.1242/dev.096628.

Habib, Shukry J., Bi-Chang Chen, Feng-Chiao Tsai, Konstantinos Anastassiadis, Tobias Meyer, Eric Betzig, and Roel Nusse. 2013. "A Localized Wnt Signal Orients Asymmetric Stem Cell Division in Vitro." *Science* 339 (6126): 1445–48. https://doi.org/10.1126/science.1231077.

Hannezo, Edouard, Jacques Prost, and Jean-Francois Joanny. 2014. "Theory of Epithelial Sheet Morphology in Three Dimensions." *Proceedings of the National Academy of Sciences of the United States of America* 111 (1): 27–32. https://doi.org/10.1073/pnas.1312076111.

Hannezo, Edouard, Colinda L. G. J. Scheele, Mohammad Moad, Nicholas Drogo, Rakesh Heer, Rosemary V. Sampogna, Jacco van Rheenen, and Benjamin D. Simons. 2017. "A Unifying Theory of Branching Morphogenesis." *Cell* 171 (1): 242–55.e27. https://doi.org/10.1016/j.cell.2017.08.026.

Hočevar Brezavšček, Ana, Matteo Rauzi, Maria Leptin, and Primož Ziherl. 2012. "A Model of Epithelial

Invagination Driven by Collective Mechanics of Identical Cells." *Biophysical Journal* 103 (5): 1069–77. https://doi.org/10.1016/j.bpj.2012.07.018.

Hufnagel, Lars, Aurelio A. Teleman, Hervé Rouault, Stephen M. Cohen, and Boris I. Shraiman. 2007. "On the Mechanism of Wing Size Determination in Fly Development." *Proceedings of the National Academy of Sciences of the United States of America* 104 (10): 3835–40. https://doi.org/10.1073/pnas.0607134104.

Humphries, Ashley Ceinwen, and Marek Mlodzik. 2017. "From Instruction to Output: Wnt/PCP Signaling in Development and Cancer." *Current Opinion in Cell Biology* 51 (December): 110–16. https://doi.org/10.1016/j.ceb.2017.12.005.

Karner, Courtney M., Rani Chirumamilla, Shigehisa Aoki, Peter Igarashi, John B. Wallingford, and Thomas J. Carroll. 2009. "Wnt9b Signaling Regulates Planar Cell Polarity and Kidney Tubule Morphogenesis." *Nature Genetics* 41 (7): 793–99. https://doi.org/10.1038/ng.400.

Krupinski, Pawel, Vijay Chickarmane, and Carsten Peterson. 2011. "Simulating the Mammalian Blastocyst--Molecular and Mechanical Interactions Pattern the Embryo." *PLoS Computational Biology* 7 (5): e1001128. https://doi.org/10.1371/journal.pcbi.1001128.

Kunimoto, Koshi, Roy D. Bayly, Eszter K. Vladar, Tyson Vonderfecht, Anna-Rachel Gallagher, and Jeffrey D. Axelrod. 2017. "Disruption of Core Planar Cell Polarity Signaling Regulates Renal Tubule Morphogenesis but Is Not Cystogenic." *Current Biology: CB* 27 (20): 3120–31.e4. https://doi.org/10.1016/j.cub.2017.09.011.

Le Garrec, Jean-François, Philippe Lopez, and Michel Kerszberg. 2006. "Establishment and Maintenance of Planar Epithelial Cell Polarity by Asymmetric Cadherin Bridges: A Computer Model." *Developmental Dynamics: An Official Publication of the American Association of Anatomists* 235 (1): 235–46. https://doi.org/10.1002/dvdy.20617.

Libby, Eric, and Paul B. Rainey. 2011. "Exclusion Rules, Bottlenecks and the Evolution of Stochastic Phenotype Switching." *Proceedings. Biological Sciences / The Royal Society* 278 (1724): 3574–83. https://doi.org/10.1098/rspb.2011.0146.

Li, Rong, and Bruce Bowerman. 2010. "Symmetry Breaking in Biology." *Cold Spring Harbor Perspectives in Biology* 2 (3): a003475. https://doi.org/10.1101/cshperspect.a003475.

Little, Melissa H. 2017. "Organoids: A Special Issue." *Development* 144 (6): 935–37. https://doi.org/10.1242/dev.150292.

Li, Yun, Julien Muffat, Attya Omer, Irene Bosch, Madeline A. Lancaster, Mriganka Sur, Lee Gehrke, Juergen A. Knoblich, and Rudolf Jaenisch. 2017. "Induction of Expansion and Folding in Human Cerebral Organoids." *Cell Stem Cell* 20 (3): 385–96.e3. https://doi.org/10.1016/j.stem.2016.11.017.

Loh, Kyle M., Renée van Amerongen, and Roel Nusse. 2016. "Generating Cellular Diversity and Spatial Form: Wnt Signaling and the Evolution of Multicellular Animals." *Developmental Cell* 38 (6): 643–55. https://doi.org/10.1016/j.devcel.2016.08.011.

Long, Jason T., Leslie Irwin, Addison C. Enomoto, Zachary Grow, Jessica Ranck, and Margaret T. Peeler. 2015. "Jun N-Terminal Kinase Activity Is Required for Invagination but Not Differentiation of the Sea Urchin Archenteron." *Genesis* 53 (12): 762–69. https://doi.org/10.1002/dvg.22898.

Lyons, Deirdre C., Stacy L. Kaltenbach, and David R. McClay. 2011. "Morphogenesis in Sea Urchin Embryos: Linking Cellular Events to Gene Regulatory Network States." *Wiley Interdisciplinary Reviews. Developmental Biology* 1 (2): 231–52. https://doi.org/10.1002/wdev.18.

Martik, Megan L., and David R. McClay. 2017. "New Insights from a High-Resolution Look at Gastrulation in the Sea Urchin, Lytechinus Variegatus." *Mechanisms of Development* 148: 3–10. https://doi.org/10.1016/j.mod.2017.06.005.

Martin-Belmonte, Fernando, and Mirna Perez-Moreno. 2011. "Epithelial Cell Polarity, Stem Cells and Cancer." *Nature Reviews. Cancer* 12 (1): 23–38. https://doi.org/10.1038/nrc3169.

Minegishi, Katsura, Masakazu Hashimoto, Rieko Ajima, Katsuyoshi Takaoka, Kyosuke Shinohara, Yayoi

Ikawa, Hiromi Nishimura, et al. 2017. “A Wnt5 Activity Asymmetry and Intercellular Signaling via PCP Proteins Polarize Node Cells for Left-Right Symmetry Breaking.” *Developmental Cell* 40 (5): 439–52.e4. https://doi.org/10.1016/j.devcel.2017.02.010.

Misra, Mahim, Basile Audoly, Ioannis G. Kevrekidis, and Stanislav Y. Shvartsman. 2016. “Shape Transformations of Epithelial Shells.” *Biophysical Journal* 110 (7): 1670–78. https://doi.org/10.1016/j.bpj.2016.03.009.

Monier, Bruno, Melanie Gettings, Guillaume Gay, Thomas Mangeat, Sonia Schott, Ana Guarner, and Magali Suzanne. 2015. “Apico-Basal Forces Exerted by Apoptotic Cells Drive Epithelium Folding.” *Nature* 518 (7538): 245–48. https://doi.org/10.1038/nature14152.

Muguruma, Keiko, Ayaka Nishiyama, Hideshi Kawakami, Kouichi Hashimoto, and Yoshiki Sasai. 2015. “Self-Organization of Polarized Cerebellar Tissue in 3D Culture of Human Pluripotent Stem Cells.” *Cell Reports* 10 (4): 537–50. https://doi.org/10.1016/j.celrep.2014.12.051.

Müller, H-Arno J., and Olaf Bossinger. 2003. “Molecular Networks Controlling Epithelial Cell Polarity in Development.” *Mechanisms of Development* 120 (11): 1231–56. https://www.ncbi.nlm.nih.gov/pubmed/14623435.

Murisic, Nebojsa, Vincent Hakim, Ioannis G. Kevrekidis, Stanislav Y. Shvartsman, and Basile Audoly. 2015. “From Discrete to Continuum Models of Three-Dimensional Deformations in Epithelial Sheets.” *Biophysical Journal* 109 (1): 154–63. https://doi.org/10.1016/j.bpj.2015.05.019.

Nagai, Tatsuzo, and Hisao Honda. 2001. “A Dynamic Cell Model for the Formation of Epithelial Tissues.” *Philosophical Magazine B* 81 (7): 699–719. https://doi.org/10.1080/13642810108205772.

———. 2009. “Computer Simulation of Wound Closure in Epithelial Tissues: Cell–basal-Lamina Adhesion.” *Physical Review E* 80 (6). https://doi.org/10.1103/physreve.80.061903.

Newman, Timothy J. 2008. “Grid-Free Models of Multicellular Systems, with an Application to Large-Scale Vortices Accompanying Primitive Streak Formation.” *Current Topics in Developmental Biology* 81: 157–82. https://doi.org/10.1016/S0070-2153(07)81005-2.

Nishimura, Tamako, Hisao Honda, and Masatoshi Takeichi. 2012. “Planar Cell Polarity Links Axes of Spatial Dynamics in Neural-Tube Closure.” *Cell* 149 (5): 1084–97. https://doi.org/10.1016/j.cell.2012.04.021.

Nissen, Silas Boye, Marta Perera, Javier Martin Gonzalez, Sophie M. Morgani, Mogens H. Jensen, Kim Sneppen, Joshua M. Brickman, and Ala Trusina. 2017. “Four Simple Rules That Are Sufficient to Generate the Mammalian Blastocyst.” *PLoS Biology* 15 (7): e2000737. https://doi.org/10.1371/journal.pbio.2000737.

Ochoa-Espinosa, Amanda, Magdalena M. Baer, and Markus Affolter. 2012. “Tubulogenesis: Src42A Goes to Great Lengths in Tube Elongation.” *Current Biology: CB* 22 (11): R446–49. https://doi.org/10.1016/j.cub.2012.04.033.

Odell, G. M., G. Oster, P. Alberch, and B. Burnside. 1981. “The Mechanical Basis of Morphogenesis. I. Epithelial Folding and Invagination.” *Developmental Biology* 85 (2): 446–62. https://www.ncbi.nlm.nih.gov/pubmed/7196351.

Osterfield, Miriam, Xinxin Du, Trudi Schüpbach, Eric Wieschaus, and Stanislav Y. Shvartsman. 2013. “Three-Dimensional Epithelial Morphogenesis in the Developing Drosophila Egg.” *Developmental Cell* 24 (4): 400–410. https://doi.org/10.1016/j.devcel.2013.01.017.

Polyakov, Oleg, Bing He, Michael Swan, Joshua W. Shaevitz, Matthias Kaschube, and Eric Wieschaus. 2014. “Passive Mechanical Forces Control Cell-Shape Change during Drosophila Ventral Furrow Formation.” *Biophysical Journal* 107 (4): 998–1010. https://doi.org/10.1016/j.bpj.2014.07.013.

Rauzi, Matteo, Ana Hočevar Brezavšček, Primož Ziherl, and Maria Leptin. 2013. “Physical Models of Mesoderm Invagination in Drosophila Embryo.” *Biophysical Journal* 105 (1): 3–10. https://doi.org/10.1016/j.bpj.2013.05.039.

Rauzi, Matteo, Uros Krzic, Timothy E. Saunders, Matej Krajnc, Primož Ziherl, Lars Hufnagel, and Maria

Leptin. 2015. “Embryo-Scale Tissue Mechanics during Drosophila Gastrulation Movements.” *Nature Communications* 6 (October): 8677. https://doi.org/10.1038/ncomms9677.

Roignot, J., X. Peng, and K. Mostov. 2013. “Polarity in Mammalian Epithelial Morphogenesis.” *Cold Spring Harbor Perspectives in Biology* 5 (2): a013789–a013789. https://doi.org/10.1101/cshperspect.a013789.

Saburi, Sakura, Ian Hester, Evelyne Fischer, Marco Pontoglio, Vera Eremina, Manfred Gessler, Sue E. Quaggin, Robert Harrison, Richard Mount, and Helen McNeill. 2008. “Loss of Fat4 Disrupts PCP Signaling and Oriented Cell Division and Leads to Cystic Kidney Disease.” *Nature Genetics* 40 (8): 1010–15. https://doi.org/10.1038/ng.179.

Schierenberg, Einhard, and Bernd Junkersdorf. 1992. “The Role of Eggshell and Underlying Vitelline Membrane for Normal Pattern Formation in the Early C. Elegans Embryo.” *Roux’s Archives of Developmental Biology: The Official Organ of the EDBO* 202 (1): 10–16. https://doi.org/10.1007/BF00364592.

Seybold, Anna, Willi Salvenmoser, and Bert Hobmayer. 2016. “Sequential Development of Apical-Basal and Planar Polarities in Aggregating Epitheliomuscular Cells of Hydra.” *Developmental Biology* 412 (1): 148–59. https://doi.org/10.1016/j.ydbio.2016.02.022.

Song, Hai, Jianxin Hu, Wen Chen, Gene Elliott, Philipp Andre, Bo Gao, and Yingzi Yang. 2010. “Planar Cell Polarity Breaks Bilateral Symmetry by Controlling Ciliary Positioning.” *Nature* 466 (7304): 378–82. https://doi.org/10.1038/nature09129.

Tamulonis, Carlos, Marten Postma, Heather Q. Marlow, Craig R. Magie, Johann de Jong, and Jaap Kaandorp. 2011. “A Cell-Based Model of Nematostella Vectensis Gastrulation Including Bottle Cell Formation, Invagination and Zippering.” *Developmental Biology* 351 (1): 217–28. https://doi.org/10.1016/j.ydbio.2010.10.017.

Tanimizu, Naoki, Atsushi Miyajima, and Keith E. Mostov. 2009. “Liver Progenitor Cells Fold up a Cell Monolayer into a Double-Layered Structure during Tubular Morphogenesis.” *Molecular Biology of the Cell* 20 (9): 2486–94. https://doi.org/10.1091/mbc.E08-02-0177.

Thompson, Darcy Wentworth, and Others. 1942. “On Growth and Form.” *On Growth and Form.* Cambridge Univ. Press. https://www.cabdirect.org/cabdirect/abstract/19431401837.

Wang, Yanshu, Tudor Badea, and Jeremy Nathans. 2006. “Order from Disorder: Self-Organization in Mammalian Hair Patterning.” *Proceedings of the National Academy of Sciences of the United States of America* 103 (52): 19800–805. https://doi.org/10.1073/pnas.0609712104.

Wu, Jun, Angel-Carlos Roman, Jose Maria Carvajal-Gonzalez, and Marek Mlodzik. 2013. “Wg and Wnt4 Provide Long-Range Directional Input to Planar Cell Polarity Orientation in Drosophila.” *Nature Cell Biology* 15 (9): 1045–55. https://doi.org/10.1038/ncb2806.

Wu, T., A. L. Manogaran, J. M. Beauchamp, and G. L. Waring. 2010. “Drosophila Vitelline Membrane Assembly: A Critical Role for an Evolutionarily Conserved Cysteine in the ‘VM Domain’ of sV23.” *Developmental Biology* 347 (2): 360–68. https://doi.org/10.1016/j.ydbio.2010.08.037.

Zegers, Mirjam M. 2014. “3D in Vitro Cell Culture Models of Tube Formation.” *Seminars in Cell & Developmental Biology* 31 (July): 132–40. https://doi.org/10.1016/j.semcdb.2014.02.016.

SUPPLEMENTARY MATERIAL

Model

In our model, we use the following potential to describe the pairwise interaction between cells

$$V_{ij} = e^{-r_{ij}} - S\, e^{-r_{ij}/\beta}, \tag{S1}$$

where r_{ij} is the center–center distance between cell i and cell j, and S is the polarity factor

$$S = \lambda_1 S_1 + \lambda_2 S_2 + \lambda_3 S_3. \tag{S2}$$

Here, λ_1, λ_2, and λ_3 are the strengths of the respective polarity terms which are given as

$$S_1 = (\hat{p}_i \times \hat{r}_{ij}) \cdot (\hat{p}_j \times \hat{r}_{ij}), \tag{S3}$$
$$S_2 = (\hat{p}_i \times \hat{q}_i) \cdot (\hat{p}_j \times \hat{q}_j), \tag{S4}$$
$$S_3 = (\hat{q}_i \times \hat{r}_{ij}) \cdot (\hat{q}_j \times \hat{r}_{ij}). \tag{S5}$$

The unit vectors $\hat{p}_i$, $\hat{p}_j$ and $\hat{q}_i$, $\hat{q}_j$ represent the apical-basal polarity and planar cell polarity of cell i and j. Throughout the paper, β is a constant which we set to 5. In order to use the Euler method, we need the gradient of V_{ij} differentiated with respect to position, $\vec{r}_i$, and the two polarities, $\vec{p}_i$ and $\vec{q}_i$:

$$\frac{dV_{ij}}{d\vec{r}_i} = e^{-r_{ij}/\beta}\left\{\gamma\,\hat{r}_{ij} - \frac{\lambda_1}{r_{ij}}\left[\left(\hat{r}_{ij}\cdot\hat{p}_j\right)\hat{p}_i + \left(\hat{r}_{ij}\cdot\hat{p}_i\right)\hat{p}_j\right] - \frac{\lambda_3}{r_{ij}}\left[\left(\hat{r}_{ij}\cdot\hat{q}_j\right)\hat{q}_i + \left(\hat{r}_{ij}\cdot\hat{q}_i\right)\hat{q}_j\right]\right\}, \tag{S6}$$

$$\frac{dV_{ij}}{d\vec{p}_i} = e^{-r_{ij}/\beta}\left\{\lambda_1\left[S_1\hat{p}_i - \hat{p}_j + \left(\hat{r}_{ij}\cdot\hat{p}_j\right)\hat{r}_{ij}\right] + \lambda_2\left[S_2\hat{p}_i - \left(\hat{q}_i\cdot\hat{q}_j\right)\hat{p}_j + \left(\hat{q}_i\cdot\hat{p}_j\right)\hat{q}_j\right]\right\}, \tag{S7}$$

$$\frac{dV_{ij}}{d\vec{q}_i} = e^{-r_{ij}/\beta}\left\{\lambda_2\left[S_2\hat{q}_i - \left(\hat{p}_i\cdot\hat{p}_j\right)\hat{q}_j + \left(\hat{p}_i\cdot\hat{q}_j\right)\hat{p}_j\right] + \lambda_3\left[S_3\hat{q}_i - \hat{q}_j + \left(\hat{r}_{ij}\cdot\hat{q}_j\right)\hat{r}_{ij}\right]\right\}. \tag{S8}$$

In order to derive Equations S6, S7, and S8, we have used the following:

$$\frac{d}{d\vec{r}_i}e^{-r_{ij}/\beta} = \frac{1}{\beta}\, e^{-r_{ij}/\beta}\,\hat{r}_{ij}, \tag{S9}$$

$$\gamma = e^{-r_{ij}(\beta-1)/\beta} - \frac{S}{\beta} + \frac{2}{r_{ij}}\left[\lambda_1\left(\hat{r}_{ij}\cdot\hat{p}_i\right)\left(\hat{r}_{ij}\cdot\hat{p}_j\right) + \lambda_3\left(\hat{r}_{ij}\cdot\hat{q}_i\right)\left(\hat{r}_{ij}\cdot\hat{q}_j\right)\right], \tag{S10}$$

$$\frac{dS_1}{d\vec{r}_i} = \frac{1}{r_{ij}}\left[\left(\hat{r}_{ij}\cdot\hat{p}_i\right)\hat{p}_j + \left(\hat{r}_{ij}\cdot\hat{p}_j\right)\hat{p}_i\right] - 2\left[\left(\hat{r}_{ij}\cdot\hat{p}_i\right)\left(\hat{r}_{ij}\cdot\hat{p}_j\right)\hat{r}_{ij}\right], \tag{S11}$$

$$\frac{dS_1}{d\vec{p}_i} = \frac{1}{p_i}\left[\hat{p}_j - \left(\hat{r}_{ij}\cdot\hat{p}_j\right)\hat{r}_{ij} - S_1\hat{p}_i\right], \tag{S12}$$

where p_i is the length of the polarity of cell i which is equal to one at all times.

Figure S1 (Related to Figure 1)

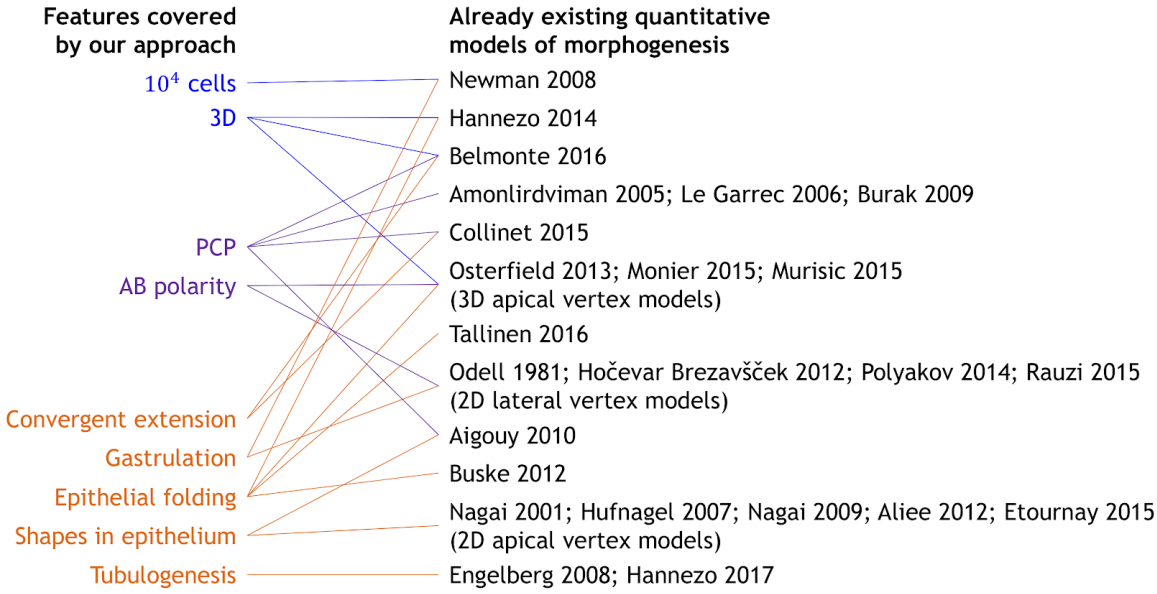

Figure S1. Overview of the existing literature on models addressing specific developmental events discussed in our work. For more references on vertex models see Alt et al. (2017).

Figure S2 (Related to Figures 2 and 3)

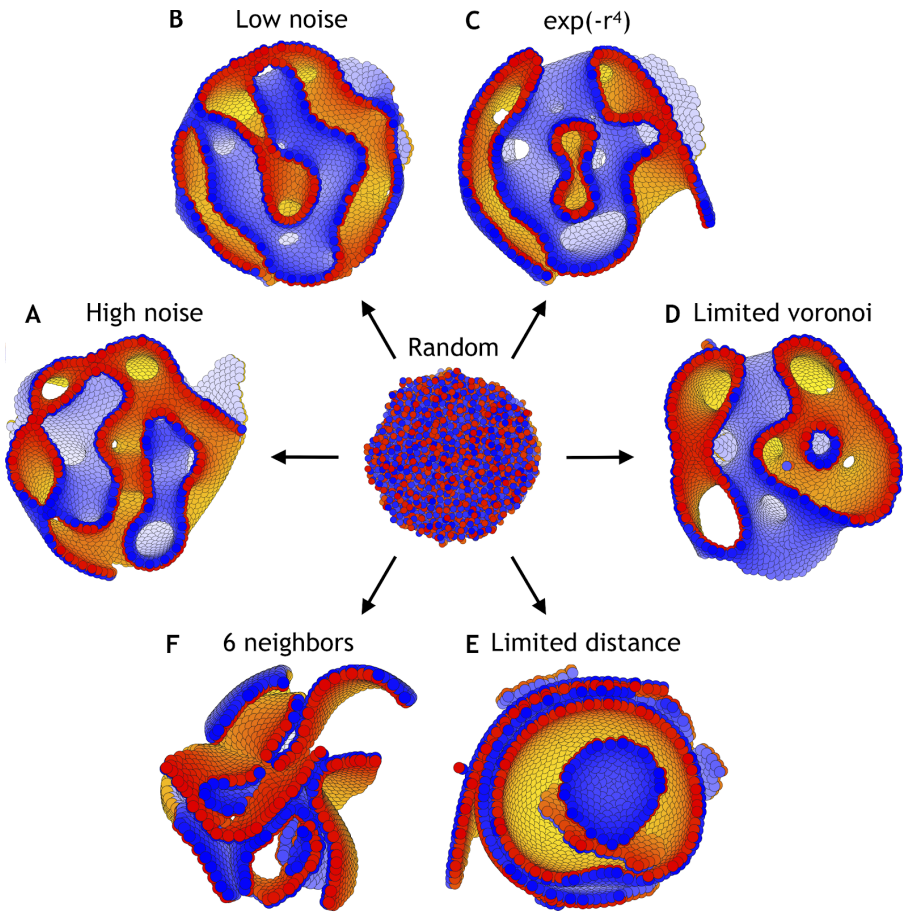

Figure S2. Dependence on noise, the shape of the physical potential, and the interaction partners. **(A)** By applying the neighborhood function as shown in Figure 2, the system reaches a metastable state with high noise ($\eta = 10^{-2}$) that is comparable to the state obtained under **(B)** low noise ($\eta = 10^{-5}$). **(C)** Changing the shape of the potential to the short range potential written in Equation 2, the system unfolds and reaches a metastable state ($\eta = 10^{-5}$). **(D)** Full Voronoi interactions with a cut-off does also lead to a metastable state, although a few cells might lose interaction with the majority of cells (cut-off at 3 shown). **(E)** Simple cut-off (and no Voronoi) does not result in metastable topologies but broken sheets on top of each other (cut-off at 2.5 shown). **(F)** When all cells always interact with their six nearest neighbors, the system breaks up and no metastable state is obtained. The initial positions and polarities are identical for all six simulations.

Figure S3 (Related to Figure 3)

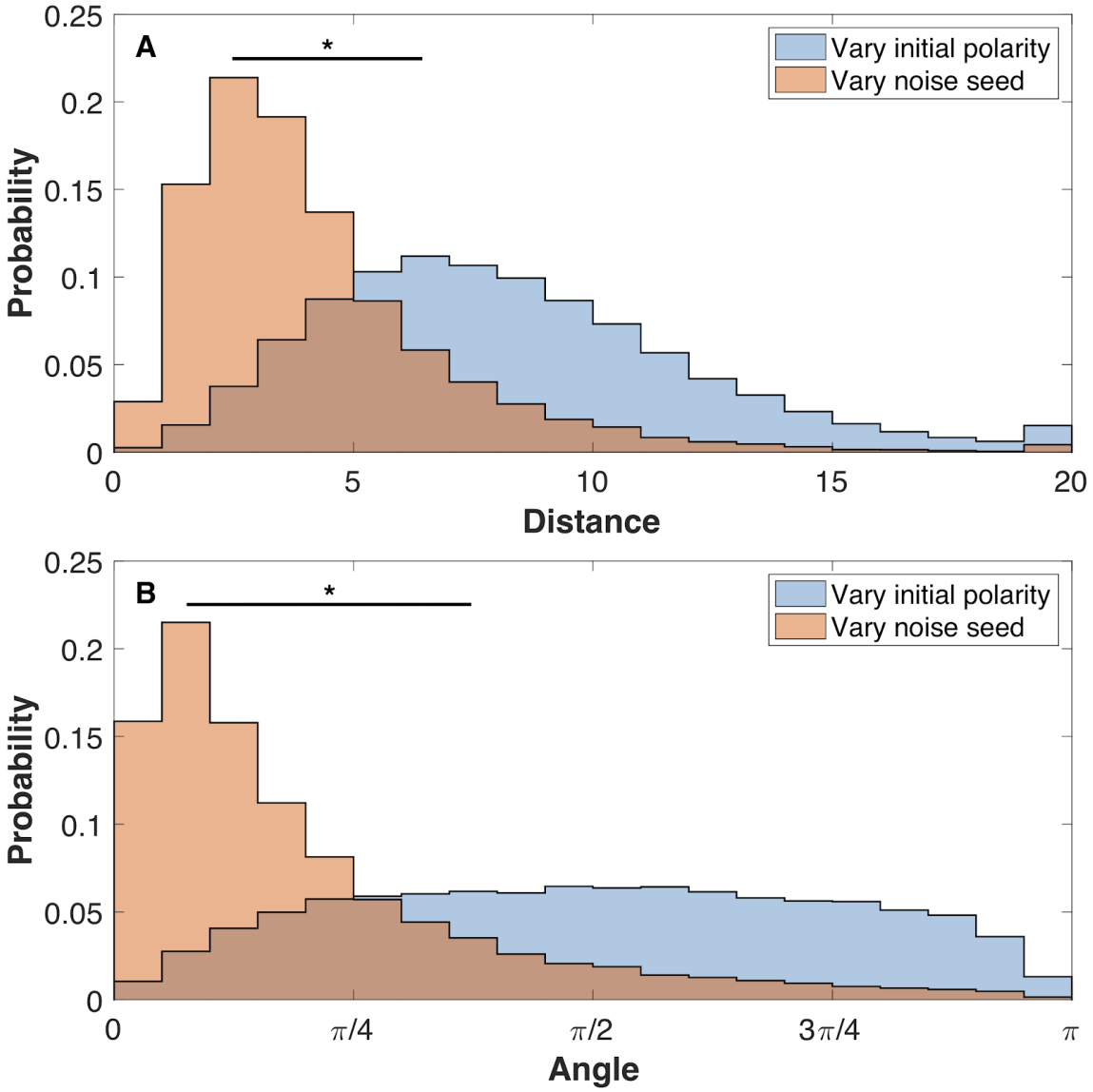

Figure S3. The final shapes are more sensitive to initial polarities than to noise. **(A)** The pairwise distance between cells for three systems with identical initial polarities but different noise and three systems with identical noise but different initial polarities. **(B)** For the same set of aggregates the angle between the pairwise polarities is calculated. The initial positions are the same for all systems. Each system has 8000 cells. Cells are pairs if they were initiated with identical position. Here, the noise level is $\eta = 10^{-5}$. Two-sample Kolmogorov-Smirnov tests showed $p < 0.001$ statistical significance (marked by *). Comparing noise levels give similar results as comparing noise seed. The initial polarities are random like in Figure 3.

Figure S4 (Related to Figure 5)

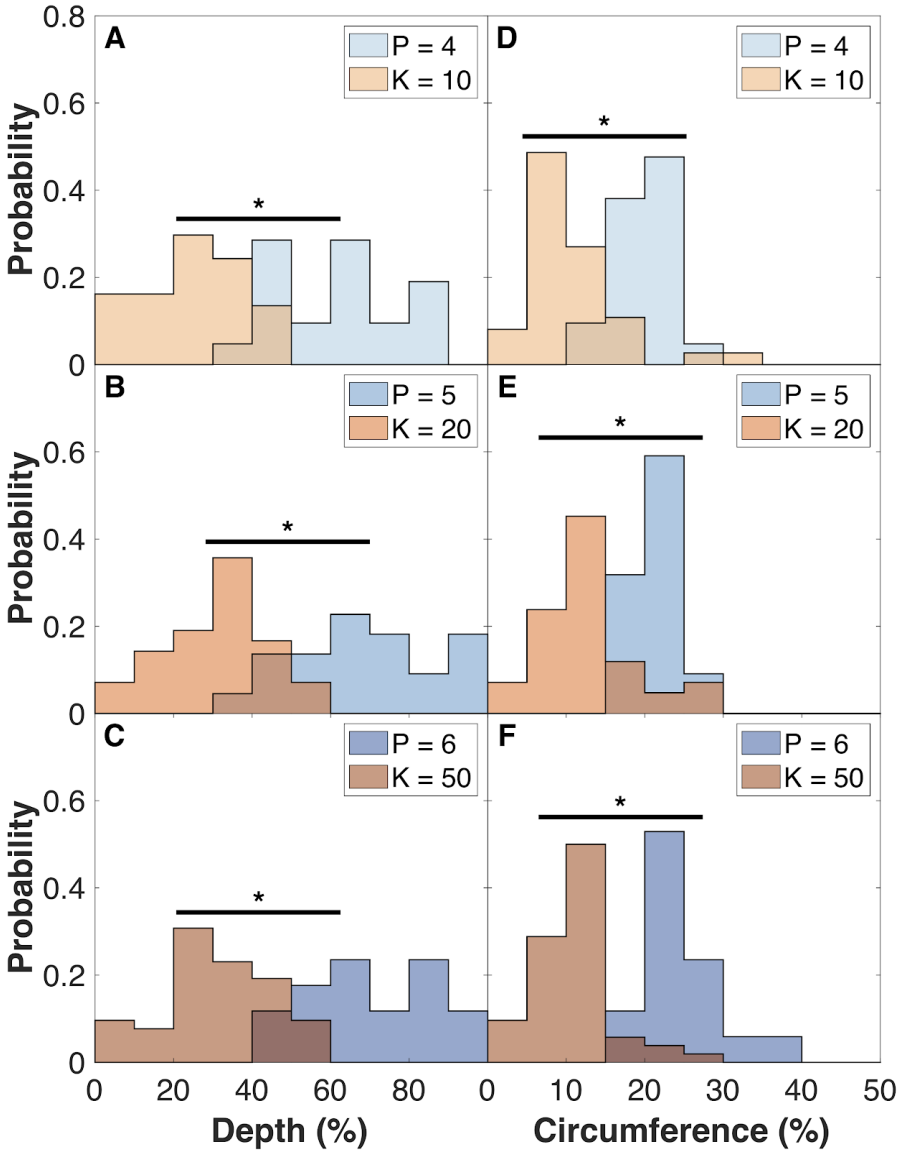

Figure S4. Organoids grown in a matrigel have deeper and longer folds compared to organoids grown with rapid cell proliferation. We fill the surface of the organoids with water until halfway between the maximum and minimum radius of the system. Then we measure the relative depth and circumference of these 'lakes'. **(A–C)** Deepest point of the 'lakes' (folds) relative to the water level. The probability of having a lake at a given depth is normalized to the number of 'lakes'. **(D–F)** Length of the 'lakes' relative to the entire circumference at this same level. Length of a lake is defined from the angle between the two cells at lake shore that are the furthest away from each other. Pressure and proliferation rate increase from upper to lower panels. Two-sample Kolmogorov-Smirnov tests showed $p < 0.001$ statistical significance (marked by *). The shown histograms are for the 16.000 cell stage, which compares to the dark blue line in Figure 5.

Figure S5 (Related to Figure 7)

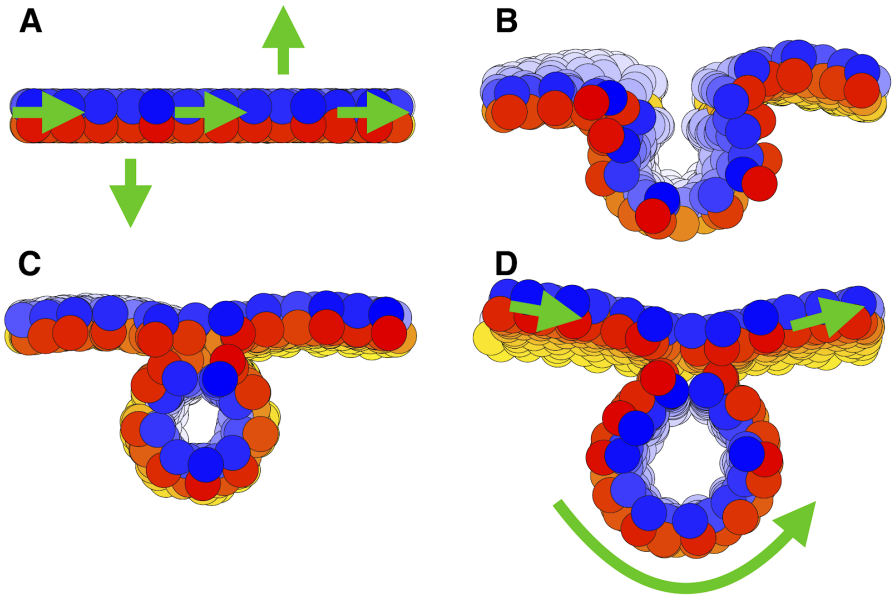

Figure S5. Planar cell polarity (PCP) enables neural plate bending and neural tube closure. **(A)** Starting with 1000 cells on a plane with apical-basal (AB) polarity, we induce PCP along the plane together with two rows where the PCP points parallel and antiparallel to AB polarity (shown with green arrows). **(B)** This enables neural plate bending and formation of the neural groove. **(C)** Continuing the simulation leads to contact of the two sides of the neural plate and hereby neural tube closure. **(D)** Finally, the system stabilizes with the neural plate on top of the neural tube. Comparing the initial stage to the final stage, the overall direction of PCP in the plate is conserved while in the tube PCP goes around an internal axis. For this simulation, we set $\lambda_2 = 0.5$ and $\lambda_3 = 0$. Turning on convergent extension (λ_3) at the final stage would allow for elongating the system along the axis going through the tube and narrowing it in another direction. The concept is similar to gastrulation in *Drosophila* and sea urchin. The latter is seen in Figure 7.

Movie 1 (Related to Figure 3)

An aggregate of 8000 cells all with apical-basal polarities initially pointing in random directions develops into a final stable complex morphology. During the simulation the polarities and positions are updated dynamically with equal speed. $\lambda_1 = 1$, and there is no planar cell polarity. Panel A shows the entire system, panel B shows half of the system viewed from the inside, while panel C shows half of the system viewed from an angle slightly above and slightly from a side. The color scheme is as described in Figure 3.

Movie 2 (Related to Figure 6)

Model of tubulogenesis. A spherical lumen consisting of 1000 cells with apical-basal polarity pointing radially out gets planar cell polarity (PCP). In equilibrium, PCP will curl around an internal axis. Depending on the relative strength of the polarities the sphere will elongate and transform to a tube with a given length and width. This movie illustrates the most extreme scenario in Figure 6 ($\lambda_1 = 0.41$, $\lambda_2 = 0.5$, and $\lambda_3 = 0.09$). Panels are similar to Movie 1. The color scheme is as described in Figure 3.

Movie 3 (Related to Figure 7)

Model of sea urchin gastrulation. Starting from a hollow sphere of 1000 cells with apical-basal polarity pointing radially out. By giving a fraction of cells planar cell polarity (PCP) pointing towards the center, the bottom flattens and invaginates. The tube forms, elongates, and connects with the upper part of the blastula when PCP has reached equilibrium curling around the axis. For more details see the caption to Figure 7. Panels are similar to Movie 1. The color scheme is as described in Figures 3 and 7.